Received: 26 October 2019 | Revised: 14 June 2020 | Accepted: 28 July 2020

DOI: 10.1002/brb3.1799

ORIGINAL RESEARCH

Brain and Behavior Open Access WILEY

A lab-on-a-chip model of glaucoma

Fatemeh Nafian[1] | Babak Kamali Doust Azad[2] | Shahin Yazdani[3,4] | Mohammad Javad Rasaee[1] | Narsis Daftarian[3,4]

[1]Department of Medical Biotechnology, Faculty of Medical Sciences, Tarbiat Modares University, Tehran, Iran

[2]Department of Electronics, School of Electrical and Computer Engineering, Tehran University, Tehran, Iran

[3]Ophthalmic Research Center, Shahid Beheshti University of Medical Sciences, Tehran, Iran

[4]Ocular Tissue Engineering Research Center, Shahid Beheshti University of Medical Sciences, Tehran, Iran

Correspondence
Mohammad Javad Rasaee, Department of Medical Biotechnology, Faculty of Medical Sciences, Tarbiat Modares University, Tehran, Iran.
Email: rasaee_m@modares.ac.ir

Abstract

Aims: We developed a glaucoma-on-a-chip model to evaluate the viability of retinal ganglion cells (RGCs) against high pressure and the potential effect of neuroprotection.

Methods: A three-layered chip consisting of interconnecting microchannels and culture wells was designed and fabricated from poly-methyl methacrylate sheets. The bottom surface of the wells was modified by air plasma and coated with different membranes to provide a suitable extracellular microenvironment. RGCs were purified from postnatal Wistar rats by magnetic assisted cell sorting up to 70% and characterized by flow cytometry and immunocytochemistry. The cultured RGCs were exposed to normal (15 mmHg) or elevated pressure (33 mmHg) for 6, 12, 24, 36, and 48 hr, with and without adding brain-derived neurotrophic factor (BDNF) or a novel BDNF mimetic (RNYK).

Results: Multiple inlet ports allow culture media and gas into the wells under elevated hydrostatic pressure. PDL/laminin formed the best supporting membrane. RGC survival rates were 85%, 78%, 70%, 67%, and 61% under normal pressure versus 40%, 22%, 18%, 12%, and 10% under high pressure at 6, 12, 24, 36, and 48 hr, respectively. BDNF and RNYK separately reduced RGC death rates about twofold under both normal and elevated pressures.

Conclusion: This model recapitulated the effects of elevated pressure over relatively short time periods and demonstrated the neuroprotective effects of BDNF and RNYK.

KEYWORDS

glaucoma, hydrostatic pressure, lab-on-a-chip, microenvironment, retinal ganglion cell

1 | INTRODUCTION

Glaucoma is a collective term used to define a group of neurodegenerative processes affecting the entire visual pathway best distinguished by progressive, irreversible destruction, and death of retinal ganglion cells (RGCs). The disease spectrum is estimated to affect more than 100 million people worldwide by the year of 2040 (Tham et al., 2014). The primary risk factor for progression and development of glaucoma is elevated intraocular pressure (IOP). IOP is regulated by the balance between aqueous humor secretion into

Fatemeh Nafian and Babak Kamali Doust Azad contributed equally to this work and should be considered as co-first authors.

the anterior chamber on one hand and its drainage via the trabecular meshwork (conventional outflow) or the uveoscleral outflow pathways on the other hand (Dawson, Ubels, & Edelhauser, 2011). The average value for normal IOP in most population-based human studies is 14–17 mmHg with 95% confidence intervals of 10–21 mmHg (Rieck, 2013).

Several experimental in vivo glaucoma models have been developed and used for study on glaucoma mechanisms. These include laser photocoagulation of the Perilimbal region (Gaasterland & Kupfer, 1974), red blood cell or microbeads injection into the anterior chamber (Quigley & Addicks, 1980), Episcleral vein obstruction (Fedorchak et al., 2014), and Episcleral vein saline injection (Morrison et al., 1997; Vecino & Sharma, 2011). Without sequential treatments, the duration of IOP elevation is transient in these models. Precise control over IOP elevation is difficult and certain problems may occur; these include intraocular inflammation, irreversible mydriasis, IOP variability, hyphema, reduced visibility of optic disks, corneal opacity, and scleral burns (Johnson & Tomarev, 2010; Rudzinski & Saragovi, 2005). While in vivo animal models are indispensable to determine what events occur in live organisms, these strategies typically involve poorly defined and uncontrollable factors and the results can be difficult to understand at cellular and molecular levels (Ishikawa, Yoshitomi, Zorumski, & Izumi, 2015).

Ishikawa et al. designed an ex vivo hydrostatic pressure model which demonstrated better retention of neuron–neuron and neuron–glial interactions in dissected eye cups (Ishikawa, Yoshitomi, Covey, Zorumski, & Izumi, 2016, 2018; Ishikawa, Yoshitomi, Zorumski, & Izumi, 2010, 2011, 2014). This model excludes the effects of ischemia and allowed studying of the direct effects of pressure on the retina. Eyecups were sunken to the bottom of a glass cylinders containing different liquid heights. Although ex vivo systems produce reliable results, there are several limitations. For example, the incubation period is limited by the duration of tissue viability because survival factors originating from axonal transport or the bloodstream are eliminated in ex vivo models.

To overcome these limitations, in vitro models have been developed using cultured cells in supporting environments to clarify glaucoma mechanisms and appear as valuable tools to evaluate the response of individual cell populations against noxious conditions and novel treatments (Dai, Zhang, Zheng, & Wang, 2018; Maurya, Agarwal, & Ghosh, 2016). These models have studied optic nerve head astrocytes, RGCs, and other types of retinal cells utilizing pressure loading systems (Agar, Li, Agarwal, Coroneo, & Hill, 2006; Lei et al., 2011; Ricard et al., 2000; Salvador-Silva et al., 2004; Tezel & Wax, 2000; Wax, Tezel, Kobayashi, & Hernandez, 2000; Yang et al., 2004). Elevation of pressure constitutes the gold standard to model ocular hypertension in vitro and has gained increasing attention in recent years. Elevated hydrostatic pressure (EHP) systems provide remarkable information on cell apoptosis, elastin synthesis, cell migration, and production of cell adhesion molecules. EHPs have provided new insights into the molecular and cellular mechanisms of glaucoma.

Recently, lab-on-a-chip (LOC) technology has been developed. This approach entails a simpler and smaller analysis platform, resulting in better temporal and spatial control of local cellular microenvironments, passive and active cell handling, less consumption of reagents, faster test results, economizing study logistics, and energy savings (Balijepalli & Sivaramakrishan, 2017). With the goal of transferring costly laboratory equipment onto small, user-friendly, easily replicable chips, LOC technology has dramatically altered many fields such as medicine, biochemistry, and biotechnology.

The aim of the present study was to design and establish a glaucoma-on-a-chip (GOC) model consisting of an EHP system coupled to a microculture system using purified primary rat RGCs. To achieve this aim, we designed pressure chips in which pressure could be modulated with the added benefits of higher speed, greater precision and finer control than previous EHP systems. We studied RGC survival under normal hydrostatic pressures (NHP) versus EHP and also compared survival of these cells when treated with a neuroprotective growth factor (brain-derived neurotrophic factor, BDNF) or a mimicry peptide, named RNYK, as a putative agonist of neurotrophic tyrosine kinase receptor type2 (NTRK2) (Nafian, Rasaee, Yazdani, & Soheili, 2018). BDNF is a well-known neuroprotectant that induces signaling through the high-affinity neurotrophin receptor (NTRK2) for neuronal survival (Kaplan & Miller, 2000). However, there are several clinical concerns about its therapeutic applications for neurodegenerative diseases. Premature BDNF can bind to the low-affinity neurotrophin receptor (p75NTR) that paradoxically mediates neuronal apoptosis (Carter, Kaltschmidt, Kaltschmidt, & Offenhauser, 1996; Roux & Barker, 2002). Therefore, at high doses and in long-term delivery, BDNF may not increase cell survival or reverse neurodegeneration. Recently, we have demonstrated that RNYK as a novel BDNF mimetic can be an alternative to circumvent these problems (Nafian, Rasaee, Yazdani, Daftarian, et al., 2018; Nafian, Rasaee, Yazdani, & Soheili, 2018). RNYK has been selected from a phage-displayed random peptide library with high-affinity binding to NTRK2 and neurotrophic activities. RNYK represses neuronal apoptosis in a NTRK2-specific manner, while having minimal lethal interactions with p75NTR. This activity has been confirmed with equal efficacy to or even better than BDNF.

2 | MATERIALS AND METHODS

2.1 | Design of a three-layered chip

In order to induce a high pressure environment to simulate glaucomatous conditions, several three-layered EHP models were designed (Figure 1). A number of morphological parameters were considered including number and location of feeding ports in the top layer (layer a), the shape of microchannels and wells in the middle layer (layer b), and surface modification for the bottom layer (layer c) of the chip. AutoCAD 2014 was used to design the layers. Some physical parameters including gas concentrations and fluid velocity profile for media at seeding/feeding time were simulated by Comsol

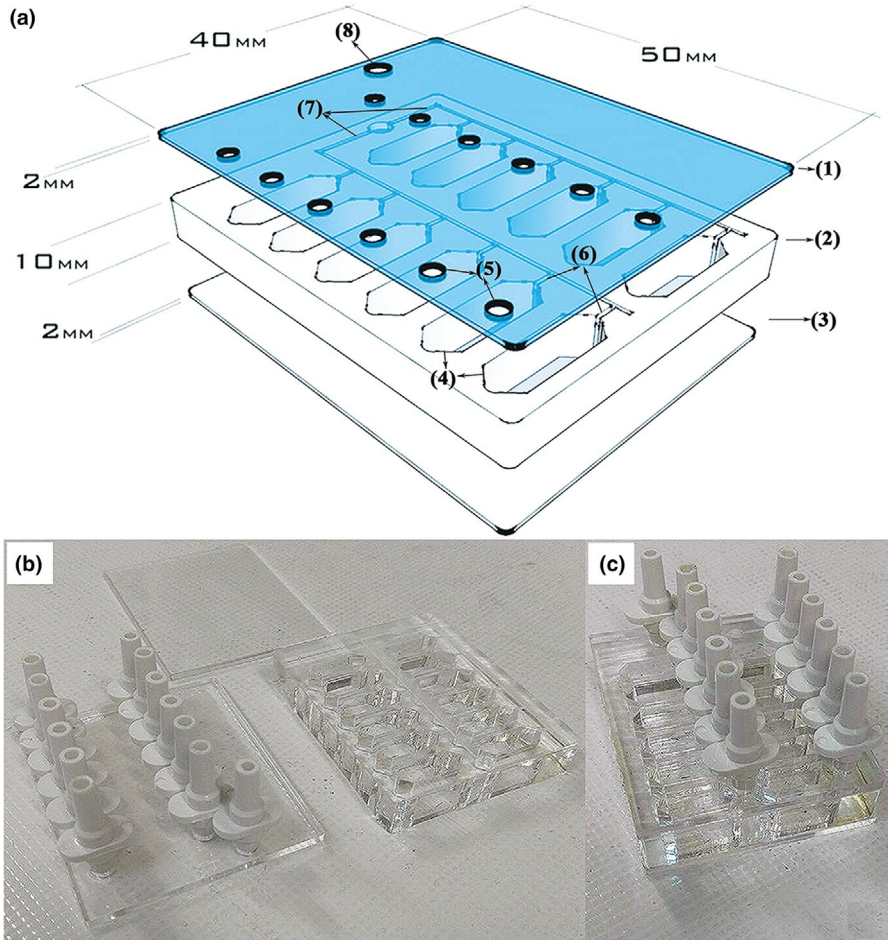

FIGURE 1 Schematic of a designed chip in AutoCAD software. (a) Three-dimensional design of layers a (1), b (2), and c (3) containing 12 wells (4), feeding ports (5), and microchannels (6), 2 main channels (7) and 1 single gas inlet (8). Layer (a) consisted of one feeding port per well and one main gas inlet. Layer B involved 12 hexagonal wells and microchannels. Layer (c) provided a surface area for cell cultures. Layers were fabricated (b) and assembled (c) to establish a complete chip

Multiphysics 5.2a software, RRID: SCR_014767, employing finite element methods. Two-dimensional incompressible Navier-Stokes equations were used along with the continuity equation to determine the liquid velocity profile of culture media throughout the fluid dynamic field at the seeding and feeding time.

$$\nabla \cdot \boldsymbol{u} = 0 \tag{1}$$

$$\rho \boldsymbol{u} \cdot \nabla \boldsymbol{u} = -\nabla p + \mu \nabla^2 \boldsymbol{u} \tag{2}$$

where $\boldsymbol{u}$ is the velocity vector, p is the pressure of injection, ρ is the density of media, and μ is the dynamic viscosity. The no-slip boundary condition was assumed at the walls. Constant velocity was specified at the inlet. The outlet was assumed to be at atmospheric pressure.

After the flow reached a steady-state condition, gas was assumed to be transported only by diffusion so that gas distribution was estimated using Fick's law (FL). Gas was released at the inlet at a specific concentration (C_0), which was monitored after a certain sampling time period. The transient two-dimensional mass transport equation is as follows:

$$\frac{\partial C}{\partial t} + \boldsymbol{u} \cdot \nabla C = D \nabla^2 C \tag{3}$$

where C is the gas concentration in the bulk, and D is the diffusion coefficient.

A novel low-cost fabrication method was established to produce the three-layered chip entirely from poly-methyl methacrylate (PMMA, Cho Chen Acrylic Co. Ltd). PMMA is the most common member of the acrylic family. The optical clarity and ability to resist environmental stress make PMMA ideal for replacing glass in light transmission applications. PMMA biocompatibility has been established through years in medicine and ophthalmology (Frazer, Byron, Osborne, & West, 2005).

2.2 | Fabrication and testing of the three-layered chip

A laser system (fiber laser, PNC laser Co. Ltd) was used to cut polymerized PMMA sheets of about 10 mm thickness for layer B and 2 mm for layers A and C. The laser processing system was equipped with a programming system (NC system), an automatic programming combining computer and CAD technology. When using the laser for fabricating channels and wells on PMMA sheet, the laser power and scanning speed were considered as main factors. Several tests were performed to explore the correct correlation between laser power and scanning speed. A 25 W-laser power and a 300 mm/s laser scanning speed were

selected to produce main channels and sub-channels on layer B. In addition, 20 W and 45 W-laser power were applied to cut PMMA sheets 10 and 2 mm in thickness respectively, at 100 mm/s laser scanning speed to make the wells and ports in layers A and B.

A thermal-solvent method was used to attach the three layers of any single chip. This method is based on dissolving PMMA in a thin layer of a solvent (isopropyl alcohol) between two PMMA substrates at 75°C for 10 min (Bamshad, Nikfarjam, & Khaleghi, 2016). Adhesion of PMMA substrates involved the following steps. First, the layers cut by the laser were rinsed in deionized water for 5 min to remove tiny debris and dried at 40°C for 10 min in an oven. Next, the solvent was added between layers B and C, which were aligned and fixed using paper clamps to avoid entrapment of air bubbles between the binding surfaces. The attached sheets were heated and finally treated with air plasma. Radiofrequency discharged plasma was generated by a dinner plasma generator from Dinner CO. at 13.6 MHz frequency and 20 W power for 10 min. The base pressure of the plasma reactor was increased to 0.35 mmHg after gas feeding. After attaching layers B and C, layer A was attached using the same method described above to complete the three-layered chip.

2.3 | Extracellular microenvironment model on modified PMMA surface

SH-SY5Y cell line (CLS Cat# 300154/p822_SH-SY5Y, RRID: CVCL_0019) which is the third sequential sub-clone of the SKN-SH human neuroblastoma cell line was purchased from the Pasteur Institute. These cells phenotypically change from neuronal type (N) to surface adherent type (S) by all-trans-retinoic acid (ATRA) treatment (Kovalevich & Langford, 2013). The cells were seeded at an initial density of 10^4 cells per cm^2 in the wells of the chip, which were precoated with one of the following membranes: collagen (0.05 mg/ml), a mixture of ploy-D-lysine (0.01 mg/ml) and laminin (0.05 mg/ml) as PDL/laminin, gelatin (1 mg/ml), and a composite nanofiber of polyacrylonitrile (PAN) and polyaniline (PANI), named PAN/PANI. The substrates were purchased from the Sigma-Aldrich Co. Ltd. When the cells were approximately 75% confluent, ATRA treatment was performed at a final concentration of 10 μM in Dulbecco's modified Eagle's medium (DMEM) (Gibco-BRL Life Technologies) supplemented with 2 mM L-glutamine, penicillin (20 U/ml), streptomycin (20 mg/ml), and 15% (by volume) fetal bovine serum (FBS) (Gibco-BRL Life Technologies) and incubated for 5 days. Cell morphology, density, and distribution were compared among different coating materials.

2.4 | Purification of RGCs and primary culture in the chip wells

Forty-eight hours before the experiment, chip surface was modified using plasma jet and exposed to UV light for 1 hr to assess successful sterilization. Then, 500 μl of PDL solution, 10 μg/ml, was added to each well for 1 hr. The wells were washed three times with sterile water and completely dried. The day before the experiment, 500 μl of laminin solution (5 μg/ml, Sigma-Aldrich) prepared in Neurobasal medium was added to each well and incubated overnight at 37°C (8% CO_2). The laminin/Neurobasal solution was replaced with 500 μl of "retinal ganglion cell media" which was prepared as follows: Neurobasal medium (Gibco-BRL Life Technologies) with 1% bovine serum albumin (BSA, Sigma-Aldrich), sodium selenite (6.7 ng/ml, Sigma-Aldrich), insulin-transferrin-selenium (ITS-G) (100×) (Thermo Fisher Scientific), progesterone (20 nM; Merck Millipore), B27 supplement (50×) (Thermo Fisher Scientific), sodium pyruvate (1 mM; Merck Millipore), L-glutamine (100×) (2 mM; Gibco-BRL Life Technologies), penicillin (20 U/ml), and streptomycin (20 mg/ml).

In accordance with the regulations of association for research in vision and ophthalmology (ARVO) for animal studies, ten postnatal day's five to seven Wistar rats (Razi Institute) were sacrificed by decapitation and then enucleated. The cornea, lens, and vitreous humor were removed, and the retina was gently lifted away using a small spatula. The retinas were stored at room temperature in 4.5 ml Hank's balanced salt solution, Ca^{2+} and Mg^{2+} free (HBSS-CMF, Sigma-Aldrich), pH 7.4. Then, 0.5 ml of trypsin (2.5%, Gibco-BRL Life Technologies) was added to the tube containing five retinas and incubated in a water bath at 37°C for 15 min where the tube was gently swirled every 5 min. The HBSS/trypsin solution was replaced by 5 ml of HBSS (containing 50 μl of DNase I 0.4%) and incubated at 37°C for 5 min. The retina was converted into a cell suspension by triturating and homogenizing the solution without introducing bubbles. The cells were centrifuged at 300 *g* for 5 min and re-suspended in 1 ml HBSS containing 0.5 mg/ml BSA. The cell suspension was filtered through a mesh filter (pore size 40 μm, BD Falcon) to yield a single-cell suspension.

After another centrifuge at 300 *g* for 5 min, the cell pellet was re-suspended in a concentration of 10^7 cells per 90 μl DPBS/BSA buffer (Dulbecco's PBS containing 0.5 mg/ml BSA). RGCs were extracted from the mixed retinal cell suspension using antibodies coupled to magnetic beads (CD90.1 MicroBeads, Miltenyi Biotec, GmbH). At first, RGCs were magnetically labeled by adding 10 μl of CD90.1 MicroBeads per 10^7 cells. The cells were incubated at room temperature for 30 min. In the next step for magnetic assisted cell sorting (MACS), the cell suspension was passed through an LS column to hold the labeled RGCs in the magnetic field of a MidiMACS system (Miltenyi Biotec). Subsequently, the adherent RGCs were rinsed with 3 ml of DPBS/BSA buffer to deplete endothelial cells and microglia. The column was removed from the separator and held over a new 15-ml tube. The adhered cells were flushed out by firmly pushing the plunger into the column and counted.

2.5 | Flow cytometry and immunocytochemistry of RGCs

In different isolation steps, cells were stained with mouse anti-CD90.1 antibody (Millipore) and goat anti-mouse IgG antibody FITC

conjugated (Santa Cruz Biotechnology, Inc.) as primary and secondary antibodies, respectively. The anti-CD90.1 antibody was added to the cell suspension at a concentration of 0.1 μg per 100 μl for 10^6 cells and incubated at 4°C for 20 min. The cells were washed three times with PBS buffer, and then 100 μl anti-mouse IgG antibody FITC conjugated was added (1:100 dilution) and incubated at room temperature for 30 min in the dark. After 3-times washing, the fluorescence emission intensity was measured using a flow cytometer. FlowJo (Tree Star, Inc.) was used to exclude dead cells from the analysis based on scatter signals. The number of cells exhibiting CD90.1 was manually counted, and the RGC percentage was calculated by determining the rate of CD90.1-positive cells relative to other ones.

Purified RGCs were cultured on a chip precoated with PDL/laminin at 37°C and 8% CO_2. After a 3-day culture, RGCs were fixed with cold methanol (−10°C) for 10 min, dried, and then blocked with 300 μl of PBS containing 1% BSA for 20 min at room temperature. The cells were incubated with 10 μl mouse anti-CD90.1 antibody (1:100 dilution) as a primary antibody overnight at 4°C. RGCs were exposed to goat anti-mouse IgG antibody FITC conjugated as a corresponding fluorescent secondary antibody (1:100 dilution) at room temperature for 1 hr in the dark. Nuclei were counterstained with 4′,6-diamidine-2′-phenylindole dihydrochloride (DAPI, Thermo Fisher Scientific) as a coloring reagent. To determine the expression of specific marker on the RGC surface (CD90.1-positive cells), several random fields were imaged under a fluorescence microscope.

2.6 | Measurement of cell viability

Retinal ganglion cells were seeded at an initial density of 10^4 cells per cm^2 in two sets of 12-well chips prior to the pressure experiment. RGCs were exposed to high hydrostatic pressures in a time-dependent manner for 6, 12, 24, 36, and 48 hr. BDNF (50 ng/ml; Thermo Fisher Scientific) and RNYK peptide (5 ng/ml) were separately applied to RGCs in one chip under NHP and the other EHP. RNYK was synthesized by Pepmic Co., Ltd with the amino acid sequence SGVYKVAYDWQH and some modifications, including N-terminal FITC labeling and C-terminal amidation. RGCs in control groups did not receive BDNF/RNYK in the same experiments. The

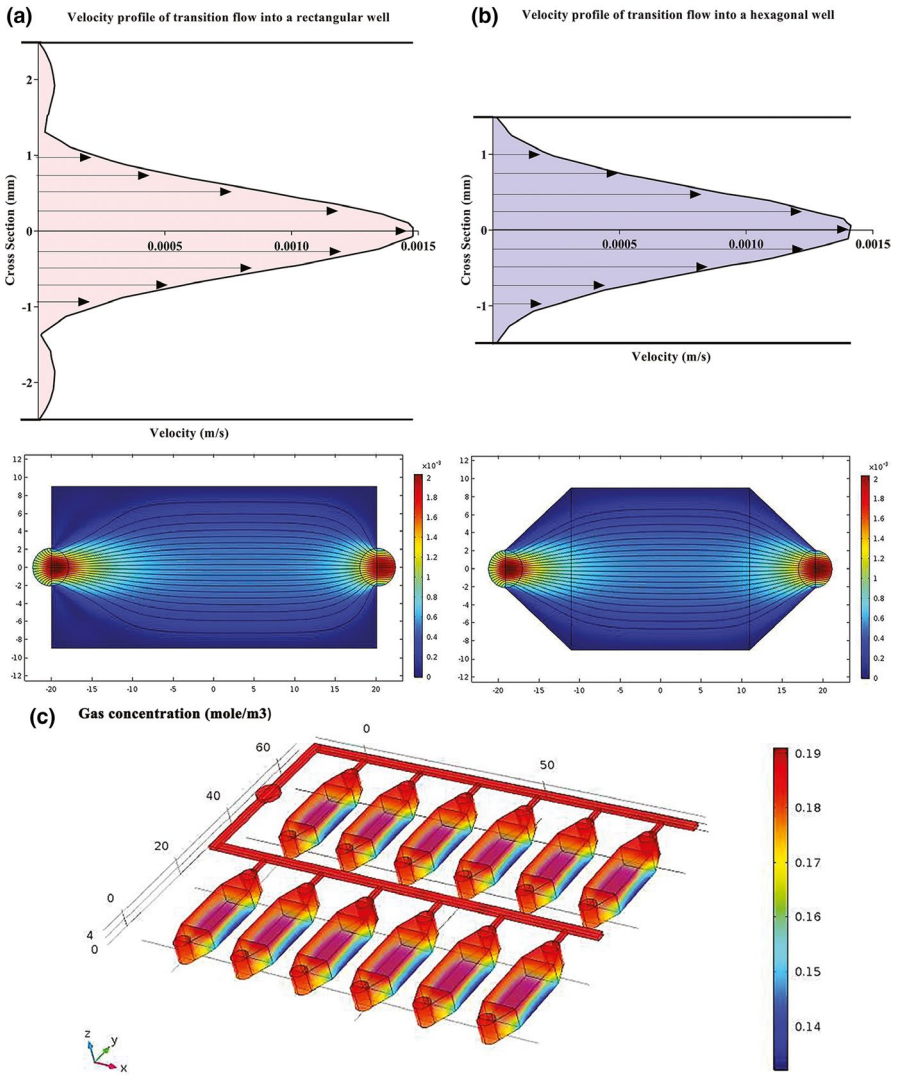

FIGURE 2 Estimated velocity profiles and gas concentration by Comsol Multiphysics software. (a) An entrance region was observed where the upstream flow entered the rectangular well. The boundary layer increased downstream, delayed the axial flow at the wall and accelerated the core flow in the center by maintaining the same flow rate. (b) The velocity profile became more even across the hexagonal well by straitening the walls at the entrance region and reducing the boundary layers at downstream (c) Gas concentration slightly changed throughout the main channels, sub-channels, and wells

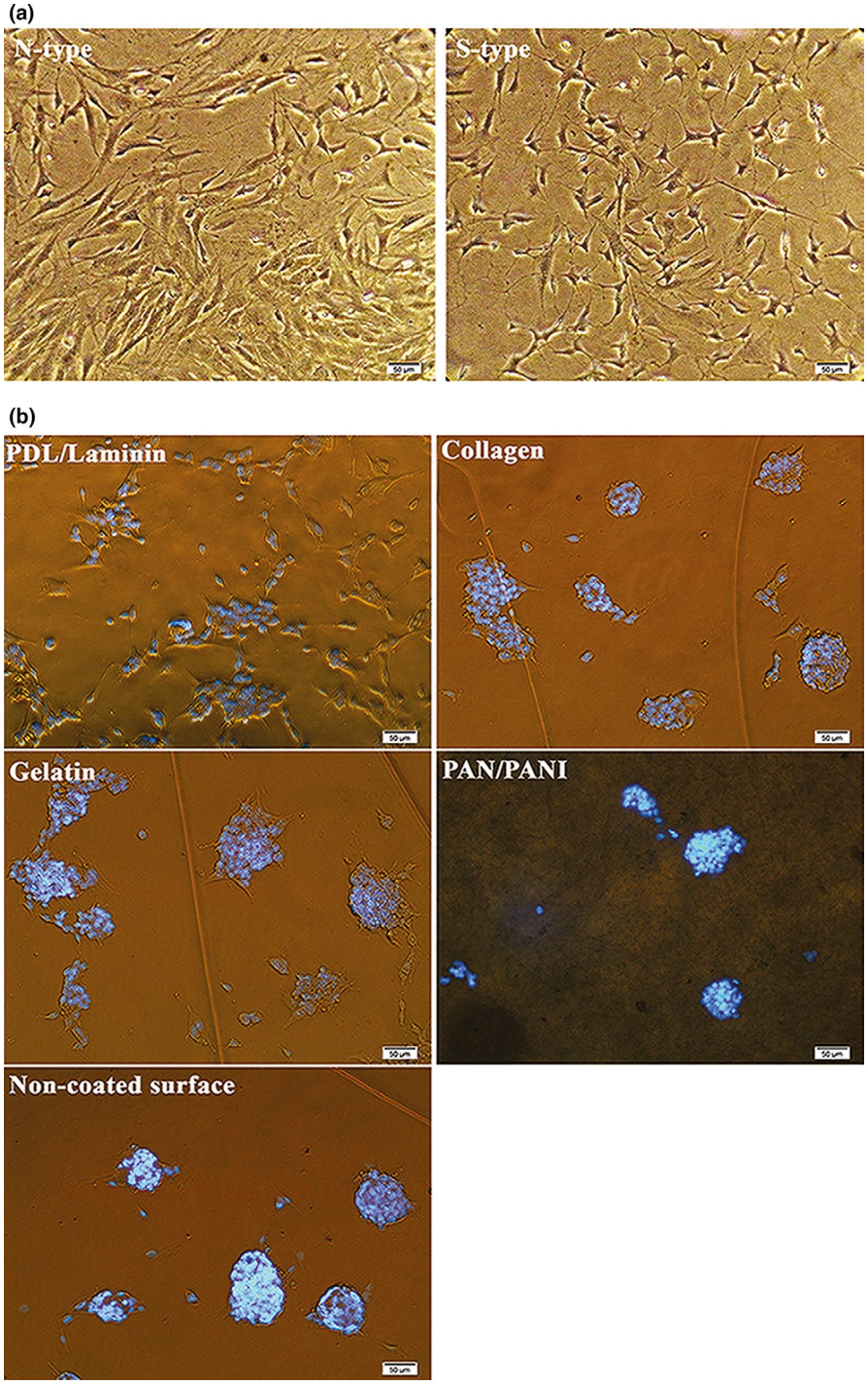

FIGURE 3 Phase-contrast images of SH-SY5Y cells. (a) Cells phenotypically changed from N-type to S-type by ATRA treatment. (b) Relatively greater number of differentiated cells oriented and aligned on different membranes compared to the naked surface as a negative control. PDL/laminin provided a physiologically optimal environment for neuronal adhesion and expansion. Scale bars: 50 μm

chip pressure was checked periodically by tonometer for fluctuations to hold the pressure level constant in each test. Cell viability was measured using 3-(4, 5-dimethylthiazol-2-yl)-2, 5-diphenyltetrazolium bromide (MTT, Sigma-Aldrich) assay for each well in the six groups. MTT solution was added to the media at a final concentration of 0.5 mg/ml and aspirated from the wells after 4 hr. The residual crystals (formazan) were dissolved in dimethyl sulfoxide (DMSO, Sigma-Aldrich), and the absorbance was measured at near 570 nm. These experiments were repeated for at least three times to check the reproducibility of biologic effects. All measured variables were described as mean ± *SD*.

2.7 | Statistical analysis

Cell viability in BDNF/RNYK treatment groups was compared with that of untreated controls under NHP and EHP. The GraphPad Prism 7.0 statistical software was employed (RRID: SCR_002798).

Significance was determined at $p < .05$ level using two-way ANOVA with Holm-Sidak's multiple comparison test.

3 | RESULTS

3.1 | Testing of the three-layered chip

The three-layered chip was designed to allow inflow of cell culture media from feeding inlets in layer A into the wells in layer B adjacent to layer C which acts the culture surface at the bottom of the wells (Figure 1). We fabricated stand-alone feeding inlets for each well to let treat culture cells within the wells in an individual manner. We initially devised two feeding ports per well in layer A (the results not shown). The drawback to this design was inappropriate surface tension leading to an uneven distribution of the culture media. We then shifted to a single feeding port at one extreme of the well and placed a gas inlet on the other extreme to allow uniform liquid distribution. Locating the feeding port at the extreme end of the well reduced shearing stress and avoided cellular detachment and necrosis in the mid-region of the well.

Based on simulation results, a hexagonal (divergent-convergent) well performed better than a rectangular well. If the cells are seeded into a rectangular well, they mainly localize in the central zone due to maximum velocity there influenced by boundary layers related to sidewalls (Figure 2a, red curve). Whereas, velocity profile became more even in a divergent-convergent input due to the reduction cross-sectional area and mitigation of boundary layer effects (Figure 2b, blue curve), resulting in a homogeneous flow velocity and cell distribution across the well at the feeding and seeding times, respectively. We designed 12 wells in each chip for simultaneously RGCs treatment with different compounds per well without any mixing of culture media or cells from one well to another via the gas channels during feeding process. The gas channels necessarily had to be interconnected to provide the same level of pressure and gas conditions to all wells within a chip. A single gas inlet was located for each chip which led to two separate main channels with six branching sub-channels (Figure 2c).

The bottom surface of the wells (layer C) was treated by air plasma to chemical modification and functionalization. This surface treatment increases surface roughness, amount of oxygen atoms, and functional hydrophilic groups (and as a result the number of polar interactions), especially the electron-donor parameters. These modifications enhance cellular adhesion which is fundamental for cell growth, migration, and differentiation.

3.2 | Extracellular microenvironment model on modified PMMA surface

All-trans-retinoic acid was added to the culture media to differentiate SH-SY5Y neuroblastoma cells into more mature, neuron-like cells. ATRA is a powerful growth inhibitor but promotes normal cellular differentiation. This low-cost procedure is easily performed as compared to primary neuronal culture and may generate a homogenous neuronal cell population. The morphology and distribution of neuron-like cells were distinguished by phase-contrast microscopy (Figure 3a). Untreated neuroblastoma cells possess large and flat cell bodies; however, neuron-like cells have branching neuronal

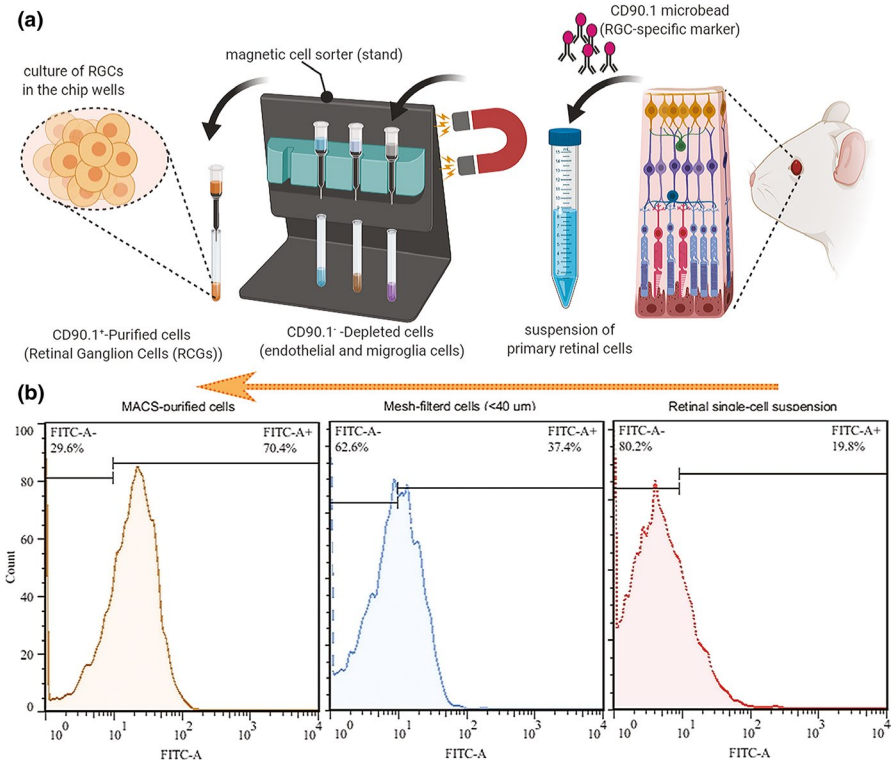

FIGURE 4 Purification of primary rat RGCs. (a) Retinal cells were isolated and converted into a cell suspension by triturating. The cell suspension was filtered through a mesh filter (>40 µm) to yield a single-cell suspension. For magnetic assisted cell sorting (MACS), the cell suspension was incubated with CD90.1 microbeads and passed through an LS column to hold the magnetically labeled cells (RGCs) in the magnetic field. The adherent RGCs were rinsed to deplete endothelial cells and microglia. The column was removed from the separator, and the adhered cells were flushed out by firmly pushing the plunger into the column and counted. (b) Flow cytometry results showed that CD90.1$^+$ cells were more purified after positive selection using MACS (orange, 70.4% purity) rather than mesh filtration (blue, 37.4%) and initial retinal single-cell suspension (red, 19.8%)

networks with smaller and round cell bodies. The neuron-like cells were cultured onto plasma-treated PMMA with different membrane coating to model the extracellular microenvironment in vitro (Figure 3b).

The cellular density was significantly more ordered with PDL/laminin coating as compared to gelatin and collagen membranes, PAN/PANI nanocomposite or nonmodified surface (negative control). The SH-SY5Y exhibited better differentiated morphology and more regular pattern of growth on the PDL/laminin membrane. Furthermore, the PDL/laminin membrane induced neurite elongation and branching, while other membranes increased cell aggregation, reminiscent of the aggregation commonly observed in undifferentiated cultures. Due to these reasons, we selected PDL/laminin surface coating for cell culture purposes in the following experiments.

3.3 | Characterization of RGCs

The steps of RGC isolation by MACS technique are summarized in Figure 4a. After isolation, flow cytometry showed high purity of RGCs, in which the percentage of RGCs was calculated by determining the ratio of CD90.1-positive cells (Figure 4b). Isolation of RGCs was initially performed using a mesh filter according to RGC cell size (>40 μm) to increase their population from a baseline of 19.8% in the single-cell retinal suspension to 37.4%. In the later stage, MACS isolated RGCs according to CD90.1 surface marker in a "yes or no" decision manner up to 70.4% purification. The RGCs exhibiting CD90.1 were also characterized using immunocytochemistry assay by above-mentioned antibodies and counterstaining with DAPI (Figure 5).

The RGCs were identified by their morphology and immunofluorescence staining characteristics. Dendrites and axons typically appear at opposing poles of the neuronal cell. On nonmodified PMMA surface, RGCs tend to form cell clusters with small to media round cell bodies with few extended fine neurites after a 10-day culture. The majority of RGCs on the modified PMMA surface exhibited uniform and round cell bodies, with neurites extending to connect to one other. At day 10, the cells developed a complex dendritic network with numerous neurites and branches (Figure 6).

3.4 | Measurement of cell viability

One set of the chips was connected to a gas tank to apply EHP at 33 mmHg, while another chip was exposed to NHP at 15 mmHg. As summarized in Figure 7a, the EHP system consisted of a compressed 8% CO_2/92% air gas tank, which was placed just outside the incubator and adjusted with both regulators for normal and ultra-low delivery pressure. Polyurethane hoses (4/8″ ID) were used to feed the gas mixture into the pressure chip through a port at the back of the incubator. A digital pressure gauge (Ashcroft, DG25; 0.5% of 0–15 psi span accuracy, ±0.1 mmHg sensitivity; relative to atmospheric pressure) was used to monitor the input pressure value. Pneumatic fittings were placed into the inlet/outlet circuits to provide tight control over gas flow. During loading, the pressure was also monitored by a sensor in the chip and kept at the 33 mm Hg with the accuracy of ±0.1 mmHg (data not shown).

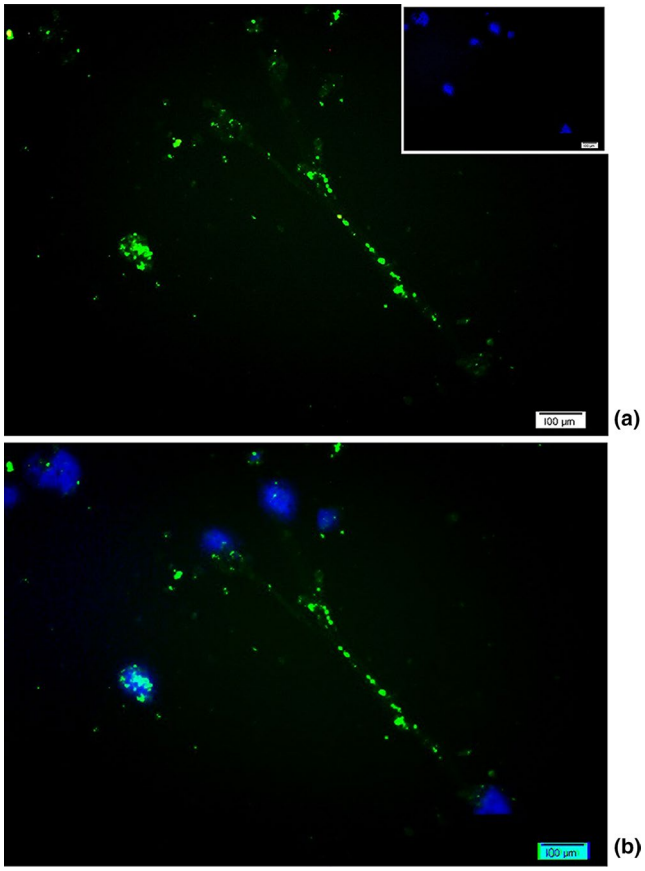

FIGURE 5 CD90.1 immunostaining of isolated rat RGCs by MACS. (a) After 3-day normal culture, RGCs continued to express the specific marker CD90.1 (green). Nuclear staining was performed using DAPI (blue). (b) The two-color merged image was produced by overlaying the original CD90.1 and DAPI images, which indicates colocalization of the axonal connections between multiple RGCs against their nucleus of cell bodies. Scale bars: 100 μm

Untreated RGCs decreased in a time-dependent manner when elevated hydrostatic pressure was applied in the chip (Figure 7b1). From 6 hr of high pressure onwards, a significant difference was observed in cell survival as compared to control cells under NHP. Cell viability results showed 85, 78, 70, 67, and 61 percent cell survival under NHP versus 40, 22, 18, 12, and 10 percent cell survival under EHP at 6, 12, 24, 36, and 48 hr ($p < .0001$), respectively. BDNF-treated RGCs demonstrated better cell survival with or without elevated pressure as compared to untreated cells. BDNF-treated RGCs showed 92, 89, 88, 83, and 80 percent viability under NHP compared with 72, 67, 64, 60, and 53 percent under EHP at 6 ($p = .0198$), 12 ($p = .0022$), 24 ($p = .0004$), 36 ($p < .0001$), and 48 ($p < .0001$) hr, respectively (Figure 7b2). RNYK provided slightly more stability than

BDNF over time. RNYK-treated RGCs showed 94, 93, 89, 87, and 86 percent viability under NHP compared with 67, 66, 63, 60, and 58 percent under EHP at 6, 12, 24, 36, and 48 hr ($p < .0001$), respectively (Figure 7b3). BDNF and RNYK treatments induced separately an approximate twofold decrease in RGC death rates as compared to untreated cells under both NHP and EHP condition.

4 | DISCUSSION

Pressure chambers are important tools to study the influence of elevated pressure on individual cell types (Aires, Ambrósio, & Santiago, 2017). Prior to employing animal models, they allow the assessment of predefined experimental conditions and evaluation of specific variables contributing to cell survival. Over the past two decades, various studies have reported significant changes in the behavior of different cells following the application of hydrostatic pressure. These changes include increased apoptosis, changes in cell morphology, and gene expression. Neuronal cells including PC12 (Agar, Yip, Hill, & Coroneo, 2000; Tök, Nazıroğlu, Uğuz, & Tök, 2014) and RGC-5 cell lines (Agar et al., 2006; Ju et al., 2007; Lee, Lu, & Madhukar, 2010; Liu et al., 2012), primary cultures of RGC (Sappington, Chan, & Calkins, 2006; Zhang et al., 2016), optic nerve head astrocytes (Liu & Neufeld, 2001, 2003; Mandal, Shahidullah, & Delamere, 2010; Miao, Crabb, Hernandez, & Lukas, 2010; Ricard et al., 2000; Salvador-Silva et al., 2004; Salvador-Silva, Ricard, Agapova, Yang, & Hernandez, 2001; Tezel, Hernandez, & Wax, 2001; Yang et al., 2004), Müller cells (Yu, Chen, et al., 2012; Yu et al., 2011; Yu, Zhong, et al., 2012), or microglial cells (Madeira et al., 2015; Sappington & Calkins, 2006, 2008), and more complex preparations such as organotypic co-cultures of the retinal cells (Obazawa et al., 2004; Osborne et al., 2015; Tezel & Wax, 2000) or eye cup preparations (Ishikawa, Yoshitomi, Zorumski, & Izumi, 2010, 2011; Reigada, Lu, Zhang, & Mitchell, 2008; Zhang et al., 2007) have been exposed to elevated pressure.

In the vast majority of glaucoma patients, IOP levels may vary from 20 to 35 mmHg. Several in vitro glaucoma models have been developed to improve the accuracy and repeatability of experiments

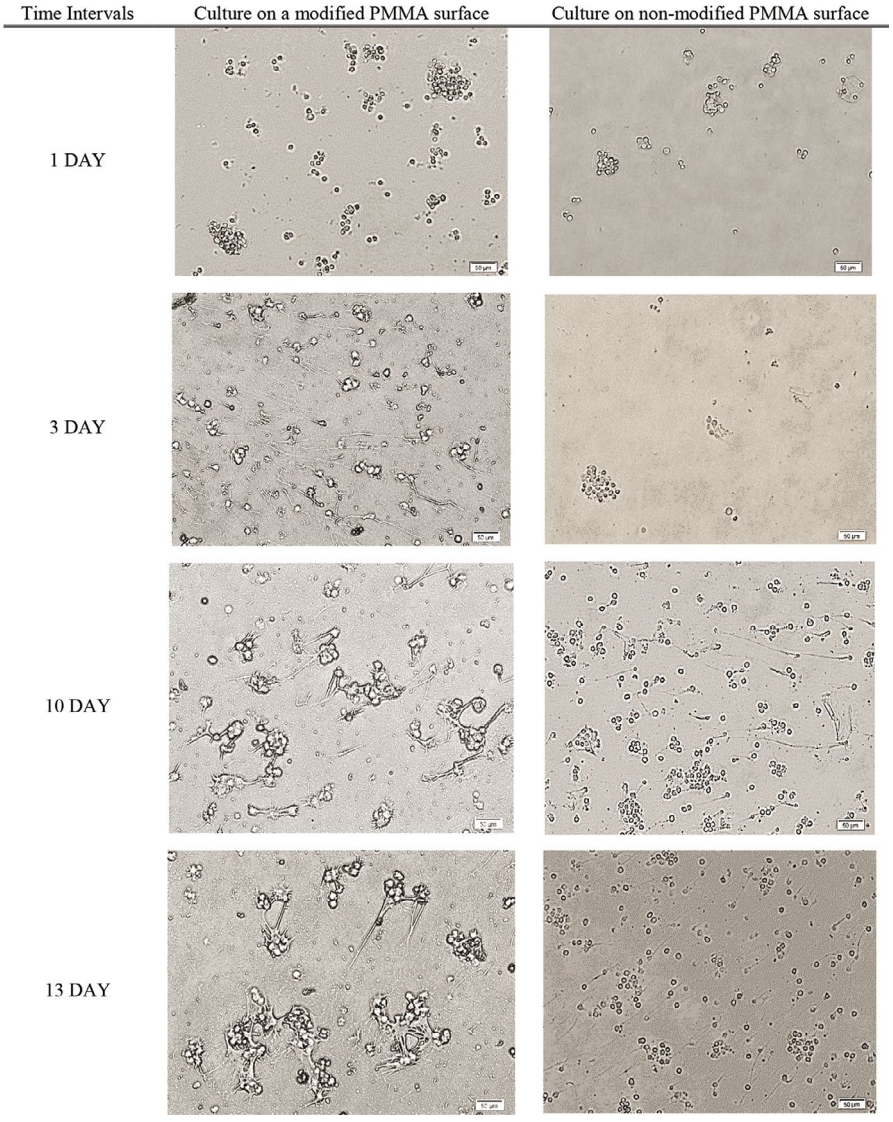

FIGURE 6 Morphological changes of primary RGCs on PMMA surface modified by plasma plus PDL/Laminin compare to nonmodified, before the pressure test. Primary RGCs formed cell clusters contained small cell bodies and few extended fine neurites on nonmodified PMMA surface. On the modified PMMA surface, RGCs exhibited uniform and round cell bodies, with neurites extending to connect to one other. At day 10, the cells developed a complex dendritic network with numerous neurites and branches. Scale bars: 50 μm

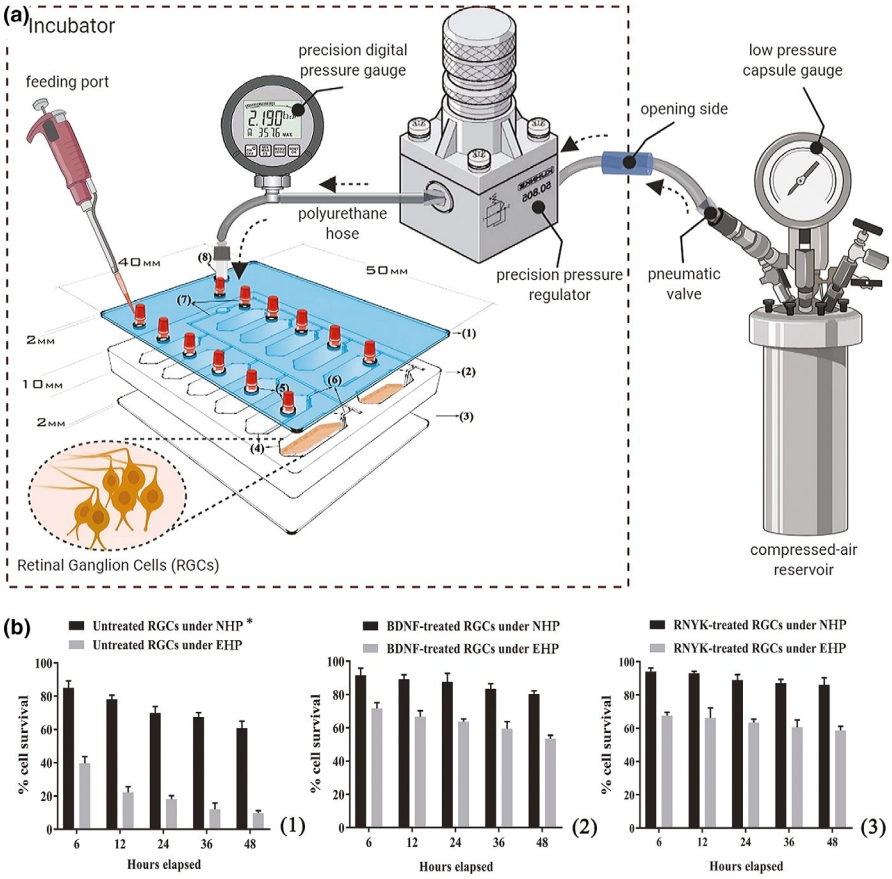

FIGURE 7 Schematic of the pressure set-up to simulate glaucomatous condition. (a) A sealed pressure chip inside the incubator was connected to a gauge and regulators placed outside by the polyurethane hoses and pneumatic valves via a side opening in the back of incubator. (b1) There was a significant decrease over time for untreated cells under EHP condition with mean difference (Mean Diff.) = 45.35, 56, 51.83, 55.43, and 51.2 (Two-way ANOVA, $N = 4$, graphs display mean ± *SD*) at 6, 12, 24, 36, and 48 hr, respectively ($p < .0001$). (b2) BDNF prevented degeneration of treated RGCs under EHP condition with Mean Diff. = 20, 22.52, 23.83, 24, and 26.7 at 6 ($p = .0198$), 12 ($p = .0022$), 24 ($p = .0004$), 36 ($p < .0001$) and 48 ($p < .0001$) hr, respectively. (B3) RNYK identically protected RGCs under EHP condition with Mean Diff. = 26.33, 26.67, 25.67, 26.33, and 27.33 at 6, 12, 24, 36, and 48 hr, respectively ($p < .0001$). *EHP, elevated hydrostatic pressure; NHP, normal hydrostatic pressure

in this pressure range. Pressurized chamber is the most commonly used model established by Kosnosky, Tripathi, and Tripathi (1995) and modified by Agar et al. (2000) to investigate cellular mechanisms In this system, a mixture of humidified gas is injected through a pressure regulator into a glass macro-chamber with ±1.5 mmHg variation. Studies using this chamber have indicated that exposure of RGC-5 cells to 30, 50, or 100 mmHg for 72, 6, or 2 hr, respectively, triggers apoptosis via oxidative stress and mitochondrial dysfunction, similar to the human condition when comparing acute glaucoma (100 mmHg) with chronic glaucoma (30 mmHg) (Agar et al., 2006; Ju et al., 2007; Liu et al., 2007, 2012; Shang et al., 2014). The second important model is a hydraulic pressurizing chamber introduced by Parkkinen et al. (1993), which compressed the internal gas phase using a hydraulic system. The device was used by Tezel and Wax (2000) to expose RGCs for 72 hr at 50 mmHg and promote neurodegeneration.

In the present study, we designed a glaucoma-on-a-chip system that provides continuous hydrostatic pressure with ±0.1 mmHg variation under a temperature-controlled environment. Our system was custom-made in agree with the pressurized chamber approach, thus, several conditions and confounding factors were carefully simulated, validated, or controlled beforehand. They consisted of fluid velocity fields, alterations in gas composition, temperature, and osmolarity to design a more stable and adjustable experiment as compared to prior in vitro studies. Our results indicated that glaucoma-on-a-chip can simulate glaucomatous conditions only when provided with a suitable microenvironment for cell-to-cell communication of RGCs. Accordingly, the PMMA surface was modified by air plasma and a thin layer of PDL/laminin to form a continuous surface of mechanical properties and uniform chemistry leading to a homogenous cell distribution. Furthermore, the evaluation of cellular mechanisms requires isolation and culture of primary RGCs. Early postnatal tissues were used to optimize RGC viability in primary cell cultures due to the limited yield and the typically postmitotic feature of these neurons in the next state. The use of RGCs in cultures on chips allowed examining a direct in vitro situation in which retinal cells maintain their microarchitecture.

Most reports investigating the degenerative effect of chronic IOP elevation have used pressures ranging from 30 mmHg (for 72 hr) to 100 mmHg (for 2 hr), as already described. In the present study, we exposed RGCs to 33 mmHg (elevated hydrostatic pressure, EHP) or 15 mmHg (normal hydrostatic pressure, NHP) for 6, 12, 24, 36, and 48 hr, with and without adding neuroprotective agents. Accordingly, cell survival of primary rat RGCs was evaluated under four different experimental conditions simulating the high pressure glaucoma (untreated RGCs under EHP), normal-tension glaucoma (untreated RGCs under NHP), neuroprotective-treated glaucoma (BDNF/RNYK-treated RGCs under EHP), and normal conditions (BDNF/RNYK-treated RGCs under NHP). Untreated groups were investigated under both NHP and EHP to determine how much damage was actually done by neurotrophin deprivation independent of elevated pressure. We also considered "untreated RGCs under NHP"

since there is no elevated IOP alerting at normal-tension glaucoma, despite the deprivation of neurotrophin. The neurotrophin hypothesis proposes that the obstruction of retrograde transport at the optic nerve head results in the loss of neurotrophic support to RGCs leading to apoptotic cell death in glaucoma (Nickells, 2012). Our results demonstrated that BDNF can maintain neuronal viability compared with untreated group under NHP. RNYK also indicated neuroprotective activities at an optimum concentration of 5 ng/ml compared with BDNF at 50 ng/ml. This observation is in agreement with our previous studies showing that RNYK could prevent neuronal degeneration of ATRA-treated SH-SY5Y with equal efficacy to or even better than BDNF (Nafian, Rasaee, Yazdani, Daftarian, et al., 2018; Nafian, Rasaee, Yazdani, & Soheili, 2018).

The negative impact of neurotrophin deprivation was compared with the insult of high pressure. In "untreated RGCs under EHP," the increase in pressure further added degenerative changes by a mechanical stress and strain in parallel to the deprivation of neurotrophic signals. Compared to normal pressure, BDNF and RNYK showed significant roles under EHP by moderating the detrimental effect of elevated pressure. They separately induced an approximate twofold decrease in RGC death rates as compared to untreated cells. In light of the findings obtained, the identified peptidomimetic compound is significant as a promising neuroprotective agent for glaucoma treatment. Also, small size of RNYK might be an advantage for drug design and synthesis in future. It is clear that in vitro models may never substitute animal studies, but they are important tools in preclinical studies. Glaucoma-on-a-chip offers the advantages of allowing controlled experimental conditions, preliminary targeting of a specific cell type or pathway involved in glaucomatous damage. More studies are needed to develop models to study RGC neurodegeneration and neuroprotection by putative agents such as neurotrophins, peptides, and other small molecules prior to assessment in animal models.

ACKNOWLEDGMENT

We are thankful to Dr Gharavi and Dr Tafreshi for technical support.

CONFLICT OF INTEREST

The authors declare that no conflict of interest exists.

AUTHOR CONTRIBUTIONS

Fatemeh Nafian and Babak Kamali Doust Azad have made substantial contributions to conception, design, and acquisitions of data. Mohammad Javad Rasaee, Narsis Daftarian, and Shahin Yazdani contributed to the analysis of data. Shahin Yazdani has been involved in writing the manuscript and given final approval of the version to be published. All authors have participated sufficiently in the work to take public responsibility for the content and agreed to be accountable for all aspects of work in ensuring that questions related to the accuracy or integrity of any part of the work are appropriately investigated and resolved.

PEER REVIEW

The peer review history for this article is available at https://publons.com/publon/10.1002/brb3.1799.

DATA AVAILABILITY STATEMENT

The data that support the findings of this study are available from the corresponding author upon reasonable request.

ORCID

Fatemeh Nafian https://orcid.org/0000-0002-0622-4086
Babak Kamali Doust Azad https://orcid.org/0000-0003-2238-6517
Shahin Yazdani https://orcid.org/0000-0002-9583-1434
Mohammad Javad Rasaee https://orcid.org/0000-0001-5674-4672
Narsis Daftarian https://orcid.org/0000-0001-5846-8739

REFERENCES

Agar, A., Li, S., Agarwal, N., Coroneo, M. T., & Hill, M. A. (2006). Retinal ganglion cell line apoptosis induced by hydrostatic pressure. *Brain Research*, *1086*(1), 191–200. https://doi.org/10.1016/j.brainres.2006.02.061

Agar, A., Yip, S. S., Hill, M. A., & Coroneo, M. T. (2000). Pressure related apoptosis in neuronal cell lines. *Journal of Neuroscience Research*, *60*(4), 495–503. https://doi.org/10.1002/(SICI)1097-4547(20000515)60:4%3C495:AID-JNR8%3E3.0.CO;2-S

Aires, I., Ambrósio, A., & Santiago, A. (2017). Modeling human glaucoma: Lessons from the in vitro models. *Ophthalmic Research*, *57*(2), 77–86. https://doi.org/10.1159/000448480

Balijepalli, A., & Sivaramakrishan, V. (2017). Organs-on-chips: Research and commercial perspectives. *Drug Discovery Today*, *22*(2), 397–403. https://doi.org/10.1016/j.drudis.2016.11.009

Bamshad, A., Nikfarjam, A., & Khaleghi, H. (2016). A new simple and fast thermally-solvent assisted method to bond PMMA–PMMA in micro-fluidics devices. *Journal of Micromechanics and Microengineering*, *26*(6), 1–12. https://doi.org/10.1088/0960-1317/26/6/065017

Carter, B. D., Kaltschmidt, C., Kaltschmidt, B., & Offenhauser, N. (1996). Selective activation of NF-kappaB by nerve growth factor through the neurotrophin receptor p75. *Science*, *272*(5261), 542–545. https://doi.org/10.1126/science.272.5261.542

Dai, M., Zhang, Q., Zheng, Z., & Wang, J. (2018). Retinal ganglion cell-conditioned medium and surrounding pressure alters gene expression and differentiation of rat retinal progenitor cells. *Molecular Medicine Reports*, *17*(5), 7177–7183. https://doi.org/10.3892/mmr.2018.8738

Dawson, D. G., Ubels, J. L., & Edelhauser, H. F. (2011). Physiology of optical media: Cornea and Sclera. In L. Leonard(Ed.), *Adler's physiology of the eye: E-book* (11th ed., pp. 119–125). Amsterdam, the Netherlands: Elsevier Health Sciences.

Fedorchak, M. V., Conner, I. P., Medina, C. A., Wingard, J. B., Schuman, J. S., & Little, S. R. (2014). 28-day intraocular pressure reduction with a single dose of brimonidine tartrate-loaded microspheres. *Experimental Eye Research*, *125*, 210–216. https://doi.org/10.1016/j.exer.2014.06.013

Frazer, R. Q., Byron, R. T., Osborne, P. B., & West, K. P. (2005). PMMA: An essential material in medicine and dentistry. *Journal of Long-Term Effects of Medical Implants*, *15*(6), 629–639. https://doi.org/10.1615/JLongTermEffMedImplants.v15.i6.60

Gaasterland, D., & Kupfer, C. (1974). Experimental glaucoma in the rhesus monkey. *Investigative Ophthalmology and Visual Science*, *13*(6), 455–457.

Ishikawa, M., Yoshitomi, T., Covey, D. F., Zorumski, C. F., & Izumi, Y. (2016). TSPO activation modulates the effects of high pressure in a rat ex vivo glaucoma model. *Neuropharmacology*, *111*, 142–159. https://doi.org/10.1016/j.neuropharm.2016.09.001

Ishikawa, M., Yoshitomi, T., Covey, D. F., Zorumski, C. F., & Izumi, Y. (2018). Additive neuroprotective effects of 24 (S)-hydroxycholesterol and allopregnanolone in an ex vivo rat glaucoma model. *Scientific Reports*, *8*(1), 1–15. https://doi.org/10.1038/s41598-018-31239-2

Ishikawa, M., Yoshitomi, T., Zorumski, C. F., & Izumi, Y. (2010). Effects of acutely elevated hydrostatic pressure in a rat ex vivo retinal preparation. *Investigative Ophthalmology and Visual Science*, *51*(12), 6414–6423. https://doi.org/10.1167/iovs.09-5127

Ishikawa, M., Yoshitomi, T., Zorumski, C. F., & Izumi, Y. (2011). Downregulation of glutamine synthetase via GLAST suppression induces retinal axonal swelling in a rat ex vivo hydrostatic pressure model. *Investigative Ophthalmology and Visual Science*, *52*(9), 6604–6616. https://doi.org/10.1167/iovs.11-7375

Ishikawa, M., Yoshitomi, T., Zorumski, C. F., & Izumi, Y. (2014). Neurosteroids are endogenous neuroprotectants in an ex vivo glaucoma model. *Investigative Ophthalmology and Visual Science*, *55*(12), 8531–8541. https://doi.org/10.1167/iovs.14-15624

Ishikawa, M., Yoshitomi, T., Zorumski, C. F., & Izumi, Y. (2015). Experimentally induced mammalian models of glaucoma. *BioMed Research International*, *2015*, 1–11. https://doi.org/10.1155/2015/281214

Johnson, T. V., & Tomarev, S. I. (2010). Rodent models of glaucoma. *Brain Research Bulletin*, *81*(2), 349–358. https://doi.org/10.1016/j.brainresbull.2009.04.004

Ju, W.-K., Liu, Q., Kim, K.-Y., Crowston, J. G., Lindsey, J. D., Agarwal, N., … Weinreb, R. N. (2007). Elevated hydrostatic pressure triggers mitochondrial fission and decreases cellular ATP in differentiated RGC-5 cells. *Investigative Ophthalmology and Visual Science*, *48*(5), 2145–2151. https://doi.org/10.1167/iovs.06-0573

Kaplan, D. R., & Miller, F. D. (2000). Neurotrophin signal transduction in the nervous system. *Current Opinion in Neurobiology*, *10*(3), 381–391. https://doi.org/10.1016/S0959-4388(00)00092-1

Kosnosky, W., Tripathi, B., & Tripathi, R. (1995). An in-vitro system for studying pressure effects on growth, morphology, and biochemical aspects of trabecular meshwork cells. *Investigative Ophthalmology and Visual Science*, *36*, 721–731.

Kovalevich, J., & Langford, D. (2013). Considerations for the use of SH-SY5Y neuroblastoma cells in neurobiology. *Neuronal Cell Culture*, *1078*, 9–21. https://doi.org/10.1007/978-1-62703-640-5_2

Lee, J. K., Lu, S., & Madhukar, A. (2010). Real-time dynamics of Ca2+, caspase-3/7, and morphological changes in retinal ganglion cell apoptosis under elevated pressure. *PLoS One*, *5*(10), e13437. https://doi.org/10.1371/journal.pone.0013437

Lei, Y., Rajabi, S., Pedrigi, R. M., Overby, D. R., Read, A. T., & Ethier, C. R. (2011). In vitro models for glaucoma research: Effects of hydrostatic pressure. *Investigative Ophthalmology and Visual Science*, *52*(9), 6329–6339. https://doi.org/10.1167/iovs.11-7836

Liu, B., Ma, X., Guo, D., Guo, Y., Chen, N., & Bi, H. (2012). Neuroprotective effect of alpha-lipoic acid on hydrostatic pressure-induced damage of retinal ganglion cells in vitro. *Neuroscience Letters*, *526*(1), 24–28. https://doi.org/10.1016/j.neulet.2012.08.016

Liu, B., & Neufeld, A. H. (2001). Nitric oxide synthase-2 in human optic nerve head astrocytes induced by elevated pressure in vitro. *Archives of Ophthalmology*, *119*(2), 240–245. https://doi.org/10.1001/pubs.Ophthalmol

Liu, B., & Neufeld, A. H. (2003). Activation of epidermal growth factor receptor signals induction of nitric oxide synthase-2 in human optic nerve head astrocytes in glaucomatous optic neuropathy. *Neurobiology of Disease*, *13*(2), 109–123. https://doi.org/10.1016/S0969-9961(03)00010-X

Liu, Q., Ju, W.-K., Crowston, J. G., Xie, F., Perry, G., Smith, M. A., … Weinreb, R. N. (2007). Oxidative stress is an early event in hydrostatic pressure–induced retinal ganglion cell damage. *Investigative Ophthalmology and Visual Science*, *48*(10), 4580–4589. https://doi.org/10.1167/iovs.07-0170

Madeira, M. H., Elvas, F., Boia, R., Gonçalves, F. Q., Cunha, R. A., Ambrósio, A. F., & Santiago, A. R. (2015). Adenosine A 2A R blockade prevents neuroinflammation-induced death of retinal ganglion cells caused by elevated pressure. *Journal of Neuroinflammation*, *12*(1), 115–128. https://doi.org/10.1186/s12974-015-0333-5

Mandal, A., Shahidullah, M., & Delamere, N. A. (2010). Hydrostatic pressure–induced release of stored calcium in cultured rat optic nerve head astrocytes. *Investigative Ophthalmology and Visual Science*, *51*(6), 3129–3138. https://doi.org/10.1167/iovs.09-4614

Maurya, N., Agarwal, N. R., & Ghosh, I. (2016). Low-dose rotenone exposure induces early senescence leading to late apoptotic signaling cascade in human trabecular meshwork (HTM) cell line: An in vitro glaucoma model. *Cell Biology International*, *40*(1), 107–120. https://doi.org/10.1002/cbin.10561

Miao, H., Crabb, A. W., Hernandez, M. R., & Lukas, T. J. (2010). Modulation of factors affecting optic nerve head astrocyte migration. *Investigative Ophthalmology and Visual Science*, *51*(8), 4096–4103. https://doi.org/10.1167/iovs.10-5177

Morrison, J. C., Moore, C., Deppmeier, L. M., Gold, B. G., Meshul, C. K., & Johnson, E. C. (1997). A rat model of chronic pressure-induced optic nerve damage. *Experimental Eye Research*, *64*(1), 85–96. https://doi.org/10.1006/exer.1996.0184

Nafian, F., Rasaee, M., Yazdani, S., Daftarian, N., Soheili, Z., & Kamali Doust Azad, B. (2018). Peptide selected by phage display increases survival of SH-SY5Y neurons comparable to brain-derived neurotrophic factor. *Journal of Cellular Biochemistry*, *120*(3), 1–11. https://doi.org/10.1002/jcb.28036

Nafian, F., Rasaee, M. J., Yazdani, S., & Soheili, Z. S. (2018). Discovery of novel peptidomimetics for brain-derived neurotrophic factor using phage display technology. *Iranian Journal of Pharmaceutical Sciences*, *14*(4), 9–20. https://doi.org/10.22034/IJPS.2018.37554

Nickells, R. W. (2012). The cell and molecular biology of glaucoma: Mechanisms of retinal ganglion cell death. *Investigative Ophthalmology and Visual Science*, *53*(5), 2476–2481. https://doi.org/10.1167/iovs.12-9483h

Obazawa, M., Mashima, Y., Sanuki, N., Noda, S., Kudoh, J., Shimizu, N., … Iwata, T. (2004). Analysis of porcine optineurin and myocilin expression in trabecular meshwork cells and astrocytes from optic nerve head. *Investigative Ophthalmology and Visual Science*, *45*(8), 2652–2659. https://doi.org/10.1167/iovs.03-0572

Osborne, A., Aldarwesh, A., Rhodes, J. D., Broadway, D. C., Everitt, C., & Sanderson, J. (2015). Hydrostatic pressure does not cause detectable changes in survival of human retinal ganglion cells. *PLoS One*, *10*(1), 1–14. https://doi.org/10.1371/journal.pone.0115591

Parkkinen, J., Ikonen, J., Lammi, M., Laakkonen, J., Tammi, M., & Helminen, H. (1993). Effects of cyclic hydrostatic pressure on proteoglycan synthesis in cultured chondrocytes and articular cartilage explants. *Archives of Biochemistry and Biophysics*, *300*(1), 458–465. https://doi.org/10.1006/abbi.1993.1062

Quigley, H. A., & Addicks, E. M. (1980). Chronic experimental glaucoma in primates. I. Production of elevated intraocular pressure by anterior chamber injection of autologous ghost red blood cells. *Investigative Ophthalmology and Visual Science*, *19*(2), 126–136.

Reigada, D., Lu, W., Zhang, M., & Mitchell, C. H. (2008). Elevated pressure triggers a physiological release of ATP from the retina: Possible role for pannexin hemichannels. *Neuroscience*, *157*(2), 396–404. https://doi.org/10.1016/j.neuroscience.2008.08.036

Ricard, C. S., Kobayashi, S., Pena, J. D., Salvador-Silva, M., Agapova, O., & Hernandez, M. R. (2000). Selective expression of neural cell adhesion

molecule (NCAM)-180 in optic nerve head astrocytes exposed to elevated hydrostatic pressure in vitro. *Molecular Brain Research*, *81*(1–2), 62–79. https://doi.org/10.1016/S0169-328X(00)00150-9

Rieck, J. (2013). The pathogenesis of glaucoma in the interplay with the immune system. *Investigative Ophthalmology and Visual Science*, *54*(3), 2393–2409. https://doi.org/10.1167/iovs.12-9781

Roux, P. P., & Barker, P. A. (2002). Neurotrophin signaling through the p75 neurotrophin receptor. *Progress in Neurobiology*, *67*(3), 203–233. https://doi.org/10.1016/S0301-0082(02)00016-3

Rudzinski, M., & Saragovi, H. U. (2005). Glaucoma: Validated and facile in vivo experimental models of a chronic neurodegenerative disease for drug development. *Current Medicinal Chemistry-Central Nervous System Agents*, *5*(1), 43–49. https://doi.org/10.2174/1568015053202796

Salvador-Silva, M., Aoi, S., Parker, A., Yang, P., Pecen, P., & Hernandez, M. R. (2004). Responses and signaling pathways in human optic nerve head astrocytes exposed to hydrostatic pressure in vitro. *Glia*, *45*(4), 364–377. https://doi.org/10.1002/glia.10342

Salvador-Silva, M., Ricard, C. S., Agapova, O. A., Yang, P., & Hernandez, M. R. (2001). Expression of small heat shock proteins and intermediate filaments in the human optic nerve head astrocytes exposed to elevated hydrostatic pressure in vitro. *Journal of Neuroscience Research*, *66*(1), 59–73. https://doi.org/10.1002/jnr.1197

Sappington, R. M., & Calkins, D. J. (2006). Pressure-induced regulation of IL-6 in retinal glial cells: Involvement of the ubiquitin/proteasome pathway and NFκB. *Investigative Ophthalmology and Visual Science*, *47*(9), 3860–3869. https://doi.org/10.1167/iovs.05-1408

Sappington, R. M., & Calkins, D. J. (2008). Contribution of TRPV1 to microglia-derived IL-6 and NFκB translocation with elevated hydrostatic pressure. *Investigative Ophthalmology and Visual Science*, *49*(7), 3004–3017. https://doi.org/10.1167/iovs.07-1355

Sappington, R. M., Chan, M., & Calkins, D. J. (2006). Interleukin-6 protects retinal ganglion cells from pressure-induced death. *Investigative Ophthalmology and Visual Science*, *47*(7), 2932–2942. https://doi.org/10.1167/iovs.05-1407

Shang, L., Huang, J.-F., Ding, W., Chen, S., Xue, L.-X., Ma, R.-F., & Xiong, K. (2014). Calpain: A molecule to induce AIF-mediated necroptosis in RGC-5 following elevated hydrostatic pressure. *BMC Neuroscience*, *15*(1), 63–70. https://doi.org/10.1186/1471-2202-15-63

Tezel, G., Hernandez, M. R., & Wax, M. B. (2001). In vitro evaluation of reactive astrocyte migration, a component of tissue remodeling in glaucomatous optic nerve head. *Glia*, *34*(3), 178–189. https://doi.org/10.1002/glia.1052

Tezel, G., & Wax, M. B. (2000). Increased production of tumor necrosis factor-α by glial cells exposed to simulated ischemia or elevated hydrostatic pressure induces apoptosis in cocultured retinal ganglion cells. *Journal of Neuroscience*, *20*(23), 8693–8700. https://doi.org/10.1523/JNEUROSCI.20-23-08693.2000

Tham, Y.-C., Li, X., Wong, T. Y., Quigley, H. A., Aung, T., & Cheng, C.-Y. (2014). Global prevalence of glaucoma and projections of glaucoma burden through 2040: A systematic review and meta-analysis. *Ophthalmology*, *121*(11), 2081–2090. https://doi.org/10.1016/j.ophtha.2014.05.013

Tök, L., Nazıroğlu, M., Uğuz, A. C., & Tök, Ö. (2014). Elevated hydrostatic pressures induce apoptosis and oxidative stress through mitochondrial membrane depolarization in PC12 neuronal cells: A cell culture model of glaucoma. *Journal of Receptors and Signal Transduction*, *34*(5), 410–416. https://doi.org/10.3109/10799893.2014.910812

Vecino, E., & Sharma, S. C. (2011). Glaucoma animal models. In R. Shimon (Ed.), *Glaucoma-basic and clinical concepts* (pp. 319–330). London, UK: InTech.

Wax, M. B., Tezel, G., Kobayashi, S., & Hernandez, M. R. (2000). Responses of different cell lines from ocular tissues to elevated hydrostatic pressure. *British Journal of Ophthalmology*, *84*(4), 423–428. https://doi.org/10.1136/bjo.84.4.423

Yang, P., Agapova, O., Parker, A., Shannon, W., Pecen, P., Duncan, J., … Hernandez, M. R. (2004). DNA microarray analysis of gene expression in human optic nerve head astrocytes in response to hydrostatic pressure. *Physiological Genomics*, *17*(2), 157–169. https://doi.org/10.1152/physiolgenomics.00182.2003

Yu, J., Chen, C., Wang, J., Cheng, Y., Wu, Q., Zhong, Y., & Shen, X. (2012). In vitro effect of adenosine on the mRNA expression of Kir 2.1 and Kir 4.1 channels in rat retinal Müller cells at elevated hydrostatic pressure. *Experimental and Therapeutic Medicine*, *3*(4), 617–620. https://doi.org/10.3892/etm.2012.457

Yu, J., Zhong, Y., Cheng, Y., Shen, X., Wang, J., & Wei, Y. (2011). Effect of high hydrostatic pressure on the expression of glutamine synthetase in rat retinal Müller cells cultured in vitro. *Experimental and Therapeutic Medicine*, *2*(3), 513–516. https://doi.org/10.3892/etm.2011.239

Yu, J., Zhong, Y., Shen, X., Cheng, Y., Qi, J., & Wang, J. (2012). In vitro effect of adenosine A2A receptor antagonist SCH 442416 on the expression of glutamine synthetase and glutamate aspartate transporter in rat retinal Müller cells at elevated hydrostatic pressure. *Oncology Reports*, *27*(3), 748–752. https://doi.org/10.3892/or.2011.1565

Zhang, S.-H., Gao, F.-J., Sun, Z.-M., Xu, P., Chen, J.-Y., Sun, X.-H., & Wu, J.-H. (2016). High pressure-induced mtDNA alterations in retinal ganglion cells and subsequent apoptosis. *Frontiers in Cellular Neuroscience*, *10*, 254–264. https://doi.org/10.3389/fncel.2016.00254

Zhang, X., Li, A., Ge, J., Reigada, D., Laties, A. M., & Mitchell, C. H. (2007). Acute increase of intraocular pressure releases ATP into the anterior chamber. *Experimental Eye Research*, *85*(5), 637–643. https://doi.org/10.1016/j.exer.2007.07.016

How to cite this article: Nafian F, Kamali Doust Azad B, Yazdani S, Rasaee MJ, Daftarian N. A lab-on-a-chip model of glaucoma. *Brain Behav*. 2020;10:e01799. https://doi.org/10.1002/brb3.1799